Estimation of snow accumulation on Samudra Tapu glacier, Western Himalaya using airborne ground penetrating radar

K. K. Singh[1,*], H. S. Negi[1], A. Kumar[2], A. V. Kulkarni[3], S. K. Dewali[1], P. Datt[1], A. Ganju[1] and S. Kumar[1]

[1]Snow and Avalanche Study Establishment, Chandigarh 160 036, India
[2]National Institute of Technology, Kurukshetra 136 119, India
[3]Divecha Centre for Climate Change, Indian Institute of Science, Bengaluru 560 012, India

In this study an airborne ground penetrating radar (GPR) is used to estimate spatial distribution of snow accumulation in the Samudra Tapu glacier (the Great Himalayan Range), Western Himalaya, India. An impulse radar system with 350 MHz antenna was mounted on a helicopter for the estimation of snow depth. The dielectric properties of snow were measured at a representative site (Patseo Observatory) using a snow fork to calibrate GPR data. The snow depths estimated from GPR signal were found to be in good agreement with those measured on ground with an absolute error of 0.04 m. The GPR survey was conducted over Samudra Tapu glacier in March 2009 and 2010. A kriging-based geostatistical interpolation method was used to generate a spatial snow accumulation map of the glacier with the GPR-collected data. The average accumulated snow depth and snow water equivalent (SWE) for a part of the glacier were found to be 2.23 m and 0.624 m for 2009 and 2.06 m and 0.496 m for 2010 respectively. Further, the snow accumulation data were analysed with various topographical parameters such as altitude, aspect and slope. The accumulated snow depth showed good correlation with altitude, having correlation coefficient varying between 0.57 and 0.84 for different parts of the glacier. Higher snow accumulation was observed in the north- and east-facing regions, and decrease in snow accumulation was found with an increase in the slope of the glacier. Thus, in this study we generate snow accumulation/SWE information using airborne GPR in the Himalayan terrain.

Keywords: Glacier, ground penetrating radar, snow accumulation, snow water equivalent.

IN the Himalaya snow and glaciers cover a large geographical area and influence climate and environment of the region. Recent studies carried out using satellite images suggest approximately 40,800 sq. km area is covered by glaciers in the Great Himalaya and Karakoram mountain ranges[1]. These glaciers are a perennial and vital source of freshwater to the countries around the Himalayan chain. In recent years, glaciers and seasonal snow cover in this region have been significantly influenced by climate change[2–7]; therefore, it is useful to monitor the spatial and temporal changes of snow thickness.

Estimation of snow thickness using field-based methods such as snow stakes, automatic sensors, etc. provides mostly point-specific information. However, ground penetrating radar (GPR), a non-destructive technique, can be used to collect both point as well as spatial distribution of snow thickness. It has been widely used in ground mode, for snow and ice thickness measurements[8–15], snowpack stratigraphic delineation[16] and to study the subsurface properties of other strata[17]. Forte *et al.*[18,19] reported the applications of GPR data in determining the density and electromagnetic (EM) wave velocity for snow, firn and ice. Colucci *et al.*[20] used GPR profiles in combination with LiDAR data to calculate the volumetric and mass variations in the body of the ice. Apart from ground mode, GPR survey has also been conducted using airborne mode. Machguth *et al.*[21] and Sold *et al.*[22] used helicopter-borne GPR on alpine glaciers to study the spatial variability of snow accumulation and compared the results with ground observations. Conway *et al.*[23] detected the bed topography of a temperate glacier using airborne GPR with a 2 MHz antenna. Recently, the airborne GPR has been used to obtain different cryospheric information (ice depth, snow layer, snow erosion due to wind, etc.) of the Antarctic region[24–26].

In the Himalaya, GPR has been mostly used in ground mode to estimate ice/glacier depth and detection of crevasses in different glaciers[27–30]. The ground-based GPR systems are difficult to operate in the rugged glaciated terrain of the Himalaya[31]. In addition, a large number of buried/hidden crevasses and hostile weather conditions pose limitations on ground-based field surveys. To overcome the above constraints, an airborne GPR technique was used by Negi *et al.*[32], which was suitable for snow depth estimation and detection of buried objects.

The snow depth information from the Himalayan glaciers is limited, though it is important for glacier health studies. Therefore, the present study is aimed at estimating

*For correspondence. (e-mail: kamal.kant@sase.drdo.in)

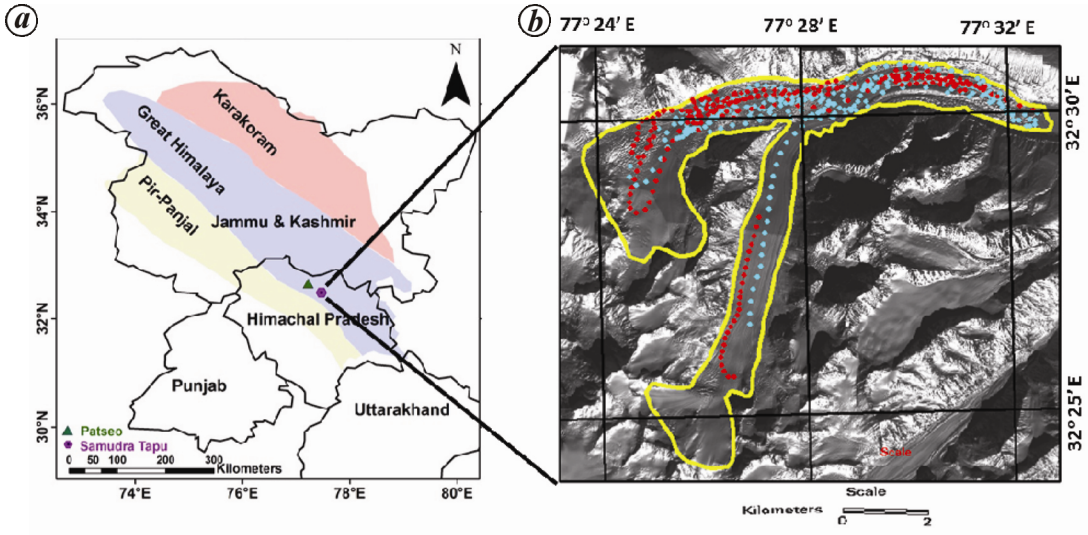

Figure 1. ***a***, Location of Patseo and Samudra Tapu glacier, study area for airborne ground penetrating radar (GPR) survey in the Great Himalaya Range of NW–Himalaya. ***b***, GPS-collected points during airborne GPR surveys in 2009 (marked with red colour) and 2010 (marked with cyan colour) overlaid on Cartosat-1 imagery of Samudra Tapu glacier.

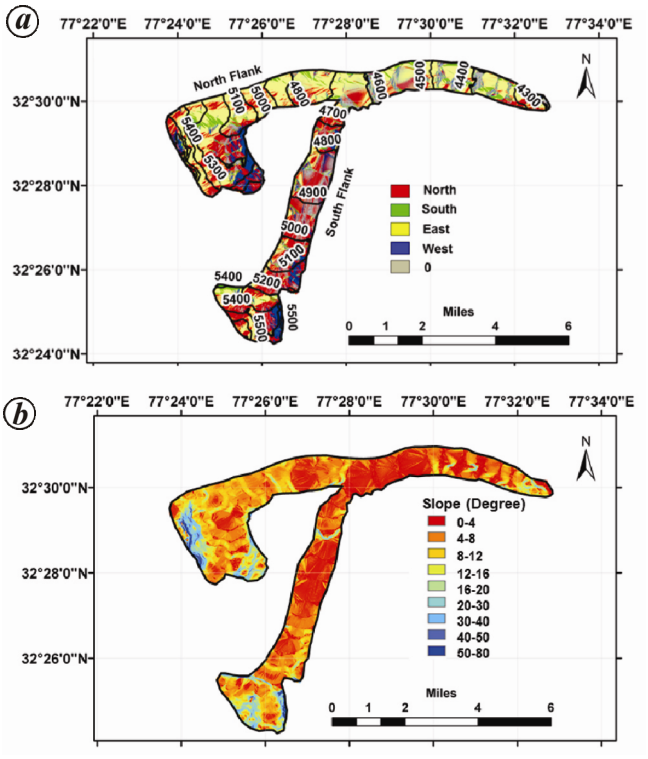

Figure 2. ***a***, Altitude and aspect information of the Samudra Tapu glacier. Contours of different height levels are marked over the glacier map. ***b***, Slope information of the glacier.

snow depth using airborne GPR. A detailed study of Samudra Tapu glacier (The Great Himalayan Range) has been carried out to estimate the snow accumulation pattern and monitor the changes in snow accumulation and snow water equivalent (SWE) for two consecutive years, i.e. 2009 and 2010. Calibration of the GPR data was performed by measuring various snowpack properties at one of the field observatories located in the same region. The survey data were further used to find the spatial variability of snow accumulation on the Samudra Tapu glacier with respect to topographic parameters, such as altitude, slope and aspect.

Study area

The study was carried out over Samudra Tapu glacier (area ~41.06 sq. km, average elevation ~4500 m) located in NW Himalaya (Figure 1). The length of the glacier is ~19 km with two nearly equal flanks (north and south). It is relatively debris-free with a large number of crevasses. A digital elevation model (DEM) of Samudra Tapu glacier was generated at 6 m spatial resolution using contour data of the Survey of India (SOI) map sheet to draw slope and aspect maps of the glacier. Figure 2 *a* shows the glacier altitude map along with aspect information. The aspect statistics of the surveyed part of the glacier shows that about half of the glacier (45%) faces east, followed by 25% towards north, 10% towards south and only 3% towards west. However, 17% of the glacier area is observed to be flat (no aspect). Further, the aspect analysis of north and south flanks of the glacier shows that the former has both north (30%) and east (45%) aspects, while the latter comprises dominantly north (58%) aspect. From the slope map of the glacier (Figure 2 *b*), the slope range was found to be generally between 0° and 10°. However, at a few places the slope was observed to vary up to ~18°.

A field site, accessible during winter was selected for the calibration of GPR-measured data. This site, Patseo (altitude: 3800 m; Figure 1 *a*), is located at ~30 km in

northwest direction from the Samudra Tapu glacier. The mean winter air temperature in this region varies between –5.9°C and –10.7°C with standard deviation (σ) ±0.8°C and the winter snowfall varies between 134 and 410 cm with $\sigma \pm 85$ cm (refs 33 and 34). Most of the slopes in this region are barren with rocky surfaces and having sparse trees at the lower altitudes. The area experiences high wind activity, relatively smaller amount of snowfall and lower average temperatures during winter[35]. Survey for snow depth estimation was carried out at this location and over Samudra Tapu glacier using airborne GPR.

Methodology

Working principle of GPR

The working principle of the GPR is based on the transmission and reception of a short EM pulse of a specified frequency from the target material. The propagation of the EM wave is governed by material properties, such as the electric permittivity, electric conductivity and magnetic permeability. Velocity of the EM wave in a medium is essential for correct estimation of depth using two-way travel time (TWT) as given in eq. (1)

$$d = (\mathrm{TWT}^* v)/2, \quad (1)$$

where d is the distance to the reflector and v is the velocity of the EM wave.

The velocity of the EM wave depends on the dielectric constant of the medium and is given by eq. (2) (refs 36, 37)

$$v = c/\sqrt{\varepsilon_r}\ , \quad (2)$$

where c is the speed of light in vacuum (0.299 m ns^{-1}) and ε_r is the dielectric constant. In the present study, we measured the dielectric constant of snow directly using a snow fork.

GPR data acquisition

In the present study, a Subsurface Interface Radar 3000 (SIR 3000; Geophysical Survey Systems, Inc.) was used for acquiring the GPR survey data. A hemispherical butterfly dipole antenna (Radarteam, Sweden) with frequency 350 MHz was used in the airborne mode. The antenna was top-shielded to ensure the transmission of EM energy in the downward direction only. The antenna (dimensions – 740 mm × 405 mm × 225 mm; weight – 6 kg) was mounted at the base of a helicopter. Figure 3 shows the mounting arrangement of the antenna. The antenna was mounted horizontally to capture the profiles at 0° incidence angle. A 10.8 V lithium-ion rechargeable battery pack was used for power supply for the operation of the entire GPR system. In order to synchronize SIR 3000 with GPS, a triggering device (TRG-817) was used (Figure 4). A marker software (GeoPointer X from Geoscanners AB, Sweden) was used to control the trigger-pulses emitted from TRG-817. The geographic information corresponding to the GPR profiles during the traverse was recorded by an RS 232 interface in a Toughbook.

Figure 3. ***a***, GPR centre frequency (350 MHz) antenna mounted beneath a helicopter for airborne data collection over Samudra Tapu glacier in India. ***b***, Air-borne GPR mounting arrangement.

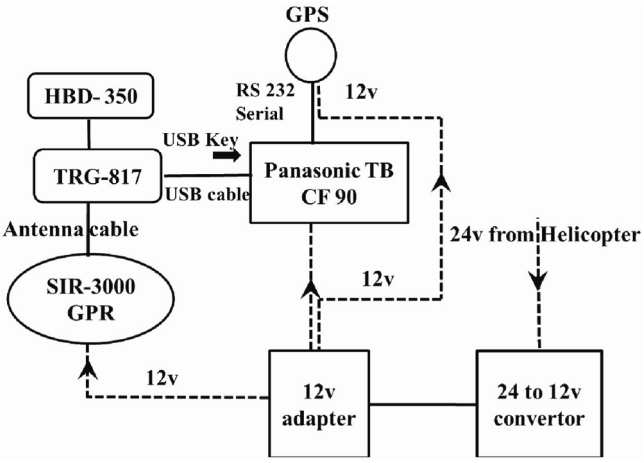

Figure 4. Block diagram of the overall air-borne GPR assembly.

During airborne survey, the helicopter height was maintained approximately at a constant level of 40 m from the ground with an average speed of ~18 m/s during the survey, so that the reflected signals could be captured within the available fixed time window of SIR 3000. For successful acquisition of GPR data in airborne mode, various parameters related to SIR-3000 need to be optimized. The size of the time window (data-capturing window), which is an important parameter, mainly depends on the antenna frequency. For lower frequencies (≤40 MHz), the time window size can be kept very large (1000 ns); however, at higher frequencies (≥1000 MHz), it can be smaller (50 ns). The window size was fixed at 200 ns for 350 MHz antenna frequency used in the present study. The GPR data were collected by keeping 512 samples in each scan with a scan rate of 64 scans per second. The stacking of six profiles was used, which resulted in an average scan rate of 10.6 scans/sec. Since the helicopter was moving at 18 m/s, the GPR takes one scan at every 1.7 m horizontally. The footprint of the antenna covers a diameter of ~7 m from a height of 40 m. A bandpass filter (100–1000 MHz) was also used along with a DC subtracting filter while taking the GPR profiles.

GPR profiles with integrated GPS positioning were collected along and across the glacier. Figure 1 *b* shows the locations of these profiles during 2009 and 2010. In each year approximately 50–55 profiles along and 20–30 profiles across the glacier were captured. To collect the geographic position coordinates, a GPS receiver Wintec G-Rays I (WBT-300) with positional accuracy better than 2.5 m was used. A manual arrangement was made to synchronize the GPR and GPS measurements, so that both instruments started measurements simultaneously. GPS measurements were taken at 10 Hz and GPR measurements were acquired at 10.6 scan/sec.

GPR data calibration using snow fork and pit measurements

The interpretation of the GPR signatures is one of the most challenging tasks. It requires information on the physical properties, particularly the dielectric constant of the medium under study. In the present study the GPR signatures were calibrated in field observatory, Patseo, during March 2009 and 2010, synchronous with the airborne surveys. The dielectric constant of the snowpack was measured using a snow fork[38]. As shown in Figure 5, it is a two-armed waveguide, which operates at ~1 GHz (ref. 39). It measures the average permittivity of a snow sample of effective length 6 cm and diameter 2 cm. Real and imaginary components of the permittivity are measured using the resonance frequency variation between air and snow. The snow fork is calibrated before each set of measurements in air. A vertical pit was dug in the snowpack of depth 1.56 m for measuring dielectric constant. The snow fork was inserted horizontally at 10 cm depth intervals from the bottom to the top. Further, the shaded wall of the pit was chosen for the measurements to avoid direct solar radiation heating of the metallic waveguides.

In addition, data on the properties of different layers of the snowpack such as thickness, density, wetness, temperature, etc. were also collected. The first snow layer from the top surface was from 1.56 to 1.20 m, and it had melt forms and rounded type of snow grains. It also had an ice layer of thickness 0.01 m at 1.25 m. The second layer was from 1.20 to 0.72 m, also composed of melt form type of snow grains. The third layer was from 0.72 to 0 m and having depth hoar type of snow grains.

Processing of GPR data

A point target on the glacier surface produces a series of echoes over a number of GPR traces along the GPR profile. The echo series appears as a hyperbola with its top indicating the presence of GPR system directly over the point target. Processing and interpretation of the airborne GPR profiles were carried out using Reflex 2D Quick Software (Sandmeier Software, Germany). In order to enhance the weak signals, a gain function was used, both during pre- and post-processing of the radar profiles. To take care of surface clutter, Still fk migration (Stolt) and

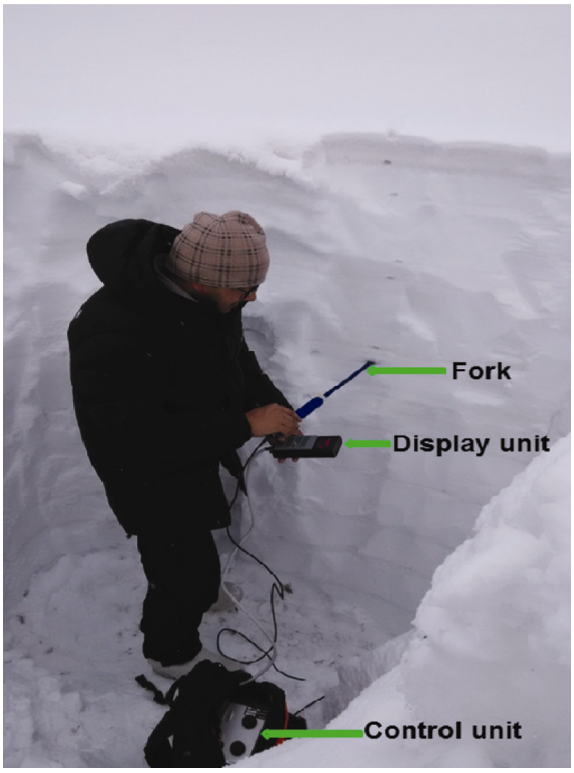

Figure 5. Snowpack data collection using a snow fork at field observatory location, Patseo (Great Himalayan Range).

background removal filters were used during collection and processing of the data. The fk migration filter was used to move all the hyperbolic reflections back to their apexes. Geographic positions of collected airborne profiles were imported in a tabular format with the help of Reflex 2D Quick software and were superimposed on the radar profiles.

In order to spatially visualize and analyse snow accumulation over the glacier surface, kriging-based geostatistical interpolation method was applied over the airborne GPR snow depth data. A semivariogram was fitted on the GPR data using a linear model for the computation of accumulated snow depth. This computed semivariogram was used to interpolate the snow accumulation distribution and to generate the interpolated snow accumulation map of the glacier. Leave-one-out cross-validation method was applied to validate the estimated snow accumulation. In this method, one of the observations is removed from the dataset and kriging is applied on the remaining[40]. The error for the excluded observation is calculated; this procedure is applied to all the observations one by one. Apart from leave-one-out cross-validation method, an independent dataset of surveyed snow depth values was used for the validation and comparison purposes.

Finally, the slope and aspect maps of the glacier were used to analyse snow cover information along the glacier terrain. The SWE over the glacier was also estimated using snow depth data from the snow accumulation map and snow density values measured at the representative field site.

Results and discussion

Calibration of GPR profile

Figure 6 *a* shows a typical radar profile having a radargram and trace window collected at the experimental site, Patseo for calibration of GPR data. This profile was taken from an airborne platform for horizontal distance of ~10 m. The dielectric constant required for accurate measurement of snow depth was measured directly using a snow fork and found to be 1.53 with $\sigma \pm 0.145$ (Table 1). The average wave velocity corresponding to this dielectric constant value was determined to be 0.241 m ns^{-1} (eq. (1)) and used during calibration experiments. In the radargram (Figure 6 *a*), the left vertical axis represents TWT in nanoseconds and the right axis shows the corresponding snow depth. In the radargram, there are two parallel intense reflections, which correspond to air–snow and snow–ground interface. Here, ground refers basically to the soil below the snowpack. The distance between these two intense lines is the measure of snow depth. The exact position of the interfaces was picked manually using both the radargram and trace window simultaneously. In this case, the upper and lower reflections were observed at ~2.1 m and ~3.62 m respectively, with a separation of 1.52 m. The snow depth was manually measured along the traversed path at multiple places and average snow depth was found to be 1.56 m. Hence the GPR-estimated snow depth is in good agreement with manually measured snow depth (absolute error of 0.04 m).

Various other reflections were also observed in the radargram, between the two main intense reflections. These less intense reflections may be attributed to the heterogeneity present in the snowpack. In the radargram, the reflection observed at 3 m depth is due to interface of depth hoar layer as confirmed during the snowpack stratigraphy measurements. In the radargram, some feeble reflections were also observed beyond 3.62 m depth, which are from deep inside the ground.

Snow accumulation on the glacier

The snow accumulation information on a glacier is useful to assess winter mass balance. Figure 6 *b* shows a radar profile collected from Samudra Tapu glacier. The

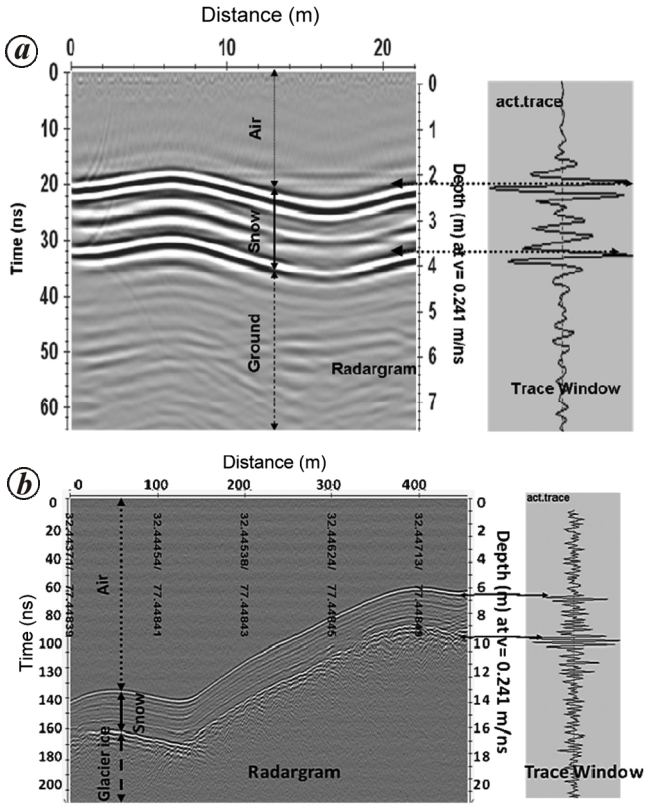

Figure 6. ***a***, Airborne GPR profile collected at Patseo (Great Himalayan Range) for calibration of GPR data for snow depth estimation. The profile was collected in conjunction with the field experiments. ***b***, Airborne GPR profile collected from Samudra Tapu glacier. Sharp reflections in radargram and trace window from two interfaces show the snow depth accumulated over glacier ice.

Table 1. Field-measured snowpack properties using a snow fork at an experimental site near Patseo (March 2010)

Snow depth (m)	Relative permittivity (ε')	Wetness (% vol.)	Snow density (kg m^{-3})	Velocity (m ns^{-1})
1.50	1.41	0.92	220	0.25
1.40	1.58	1.54	243	0.24
1.30	1.47	0.24	238	0.25
1.20	1.5	0.74	235	0.24
1.10	1.76	1.36	335	0.23
1.00	1.69	1.46	299	0.23
0.90	1.78	1.36	343	0.22
0.80	1.78	1.64	334	0.22
0.70	1.53	0.62	253	0.24
0.60	1.37	0.35	190	0.26
0.50	1.43	0.84	199	0.25
0.40	1.38	0.94	167	0.26
0.30	1.41	0.35	206	0.25
0.20	1.44	0.97	200	0.25
0.10	1.42	1.80	147	0.25
Average	1.53	1.00	241	0.241

accumulated snow on the glacier surface was estimated using the methodology discussed in the previous section. Here the sharp reflections in the radargram correspond to air–snow and snow–ice interfaces. It can be seen from Figure 6 *b* that there are continuous feeble reflections between the two dominant intense reflections, which correspond to different snow layers present in the accumulated snow over the glacier surface. The EM wave velocity (0.241 m ns^{-1}) estimated during the calibration process of the GPR profile was used to estimate the accumulated snow depth over the glacier.

Further the spatial distribution of accumulated snow cover over the glacier was estimated using geostatistical interpolation technique which was applied to GPR data. The computed semivariogram was modelled using a linear model, which gave slope as 2.11 and intercept as 0.24 (Figure 7). The linear model suggests a spatial trend in the snow-cover distribution. Figure 8 shows the interpolated snow accumulation map. The accumulation and ablation zones of the glacier identified using equilibrium line altitude (ELA, 4950 m) are also shown in the figure. To estimate ELA, annual snow line of the glacier was monitored at the end of the ablation period in each year between 2004 and 2010 using the images of Linear Imaging Self Scanning Sensor (LISS-III) on-board the Indian Remote Sensing Satellite (IRS 1C/1D).

Snow accumulation on the glacier was observed to increase with an increase in glacier altitude. The accumulation of snow varies from 2.25 to 4.34 m in the accumulation zone, and 0.72 to 2.25 m in the ablation zone for year 2010 (Figure 8). The variation of accumulated snow with elevation shows that for the accumulation zone it is 3.8 m km^{-1} and for the ablation zone it is 1.7 m km^{-1} for the same year. The interpolated snow accumulation map shows high spatial variability of accumulated snow on the glacier.

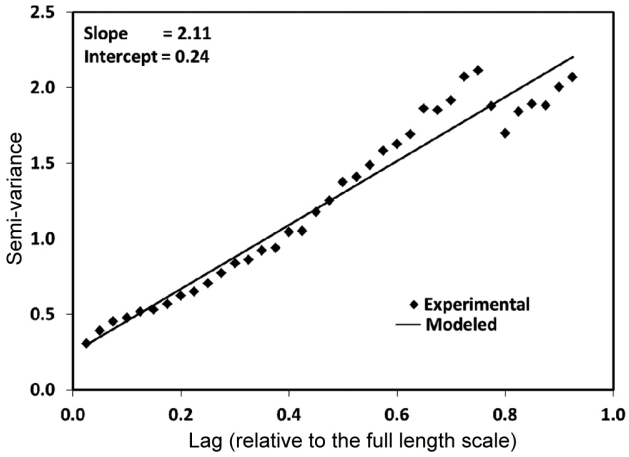

Figure 7. Experimental and modelled semivariogram estimated using the airborne GPR data acquired from Samudra Tapu glacier. The slope of the modelled linear semivariogram is 2.11 and intercept is 0.24.

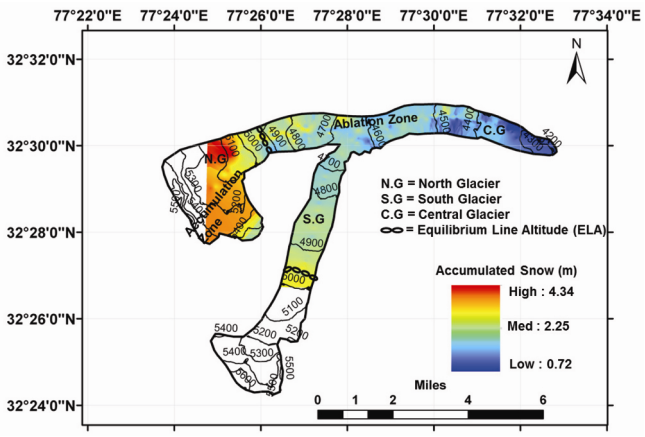

Figure 8. Spatial snow accumulation map of Samudra Tapu glacier for 2010 using snow accumulation data acquired by airborne GPR. The snow accumulation variation is shown for accumulation/ablation zone and for north/south/common glacier.

The GPR observed and interpolated snow accumulation values were found to be in close agreement with each other (Figure 9). Mean bias was found to be –0.04 m, which indicates that the interpolated values underestimate the observed snow depth. The mean absolute error (MAE) and root mean square error (RMSE) of interpolated snow accumulation were found to be 0.34 and 0.41 m respectively. Statistically significant correlation (correlation coefficient = 0.77, significant at 1%) was found between interpolated and observed snow accumulation.

Snow accumulation over the glacier varies with terrain topography. Detailed analysis of snow accumulation variation with altitude, aspect and slope is given later in the article.

Uncertainties in snow accumulation on glacier: The varying values of dielectric constant estimated from different empirical relations will affect the accuracy of the generated snow accumulation map. In order to estimate uncertainties in accumulated snow depth values retrieved on the glacier, different wave velocities derived from dielectric constant values were applied on the airborne GPR data. Assuming the snow is dry, using a wave velocity[41] in the snowpack of 0.237 m ns^{-1}, results in a difference of 2.17% from the snow accumulation values as estimated using the calculated velocity, i.e. 0.241 m ns^{-1}. However, a velocity of 0.219 m ns^{-1} as given by Ambach and Denoth[42] corresponding to the manual measured density (290 kg m^{-3}) of the snowpack, gives a large difference of about 7.6% in the estimated snow accumulation values.

Snow accumulation with altitude: Figure 10 provides an analysis of snow accumulation along with altitude variations for 2009 and 2010. The altitude of the north flank (north glacier), south flank (south glacier) and central glacier varies from 4682 to 5175 m, 4629 to 4969 m and 4240 to 4533 m respectively. The accumulated snow depth was observed to increase with increase in the glacier altitude on both the flanks (Figure 10 *a*, *d*, *e*) and in the central glacier (Figure 10 *b* and *c*). The accumulated snow depth varied from 1.16 to 4.34 m in the north flank, 1.68 to 2.94 m in the south flank and 0.87 to 2.61 m in the central glacier during the study period. More precipitation (snow) at higher altitude could be attributed to the orographic effect, which results in an increase in snow accumulation with elevation[43–48]. Correlation coefficients of accumulated snow depth on the north flank, south flank and central glacier with the altitude were found to be 0.78, 0.84 and 0.57 respectively (significant at 1% significance level). Large variations were observed in the accumulated snow depth on the north flank with $\sigma \pm 0.61$ m as compared to the south flank ($\sigma \pm 0.31$ m). This large variation in snow depth could be supported by the topography of the glacier, as the north flank is more uneven in comparison to the south flank (Figure 2 *a* and *b*).

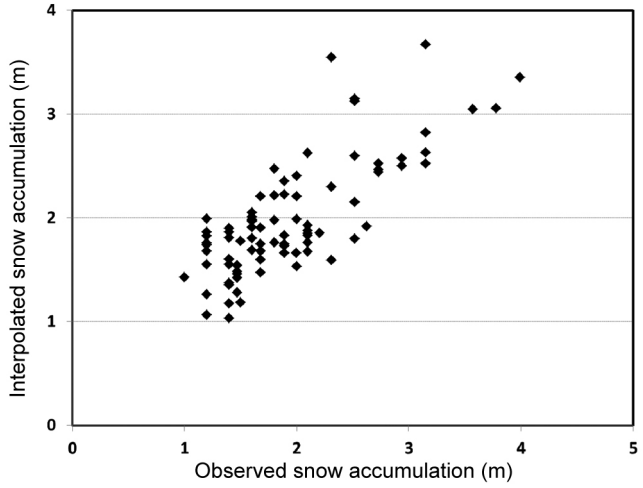

Figure 9. Comparison of airborne GPR-estimated snow accumulation values with interpolated snow accumulation values obtained after applying kriging technique.

Snow accumulation with aspect: Figure 11 shows the analysis of aspect-wise snow accumulation over the glacier. In this analysis, 53 snow depth data points having the same altitude from north, east and south facing slopes of the glacier were taken. As the area of west aspect slopes was less (3%) in the surveyed region, we found only eight snow depth data points. Due to the small number of data points, the analysis with respect to west aspect could not be performed. The frequency distribution of the highest snow accumulation values corresponding to each similar altitude for all the three aspects was analysed. It was observed that out of 53 data points, ~47% lay in the north aspect, 40% in the east aspect and only 13% in the south aspect. This shows that the snow deposited on the north and east aspects has relatively higher thickness compared to that on south aspect at the same altitude (Figures 2 and 11). The north and east aspects in general receive less radiations during the winter in northern hemisphere, which may cause low settlement/ablation in these areas. However, higher amount of solar radiation in the south aspect may be attributed to faster metamorphism and higher settlement, which lead to relatively shallow snowpack. Jain *et al.*[49] have also reported similar observations for snow accumulation in different aspects.

Snow accumulation with slope: Figure 12 shows the variation of accumulated snow with slope for different altitude ranges of the glacier. The altitude of the surveyed area varies between 4300 and 5100 m. This elevation range of the glacier was divided into four different classes, i.e. 4300–4500 m, 4500–4700 m, 4700–4900 m and 4900–5100 m. Mean snow accumulation for each slope was calculated from the points within an altitude range. Mean snow accumulation depth was found to

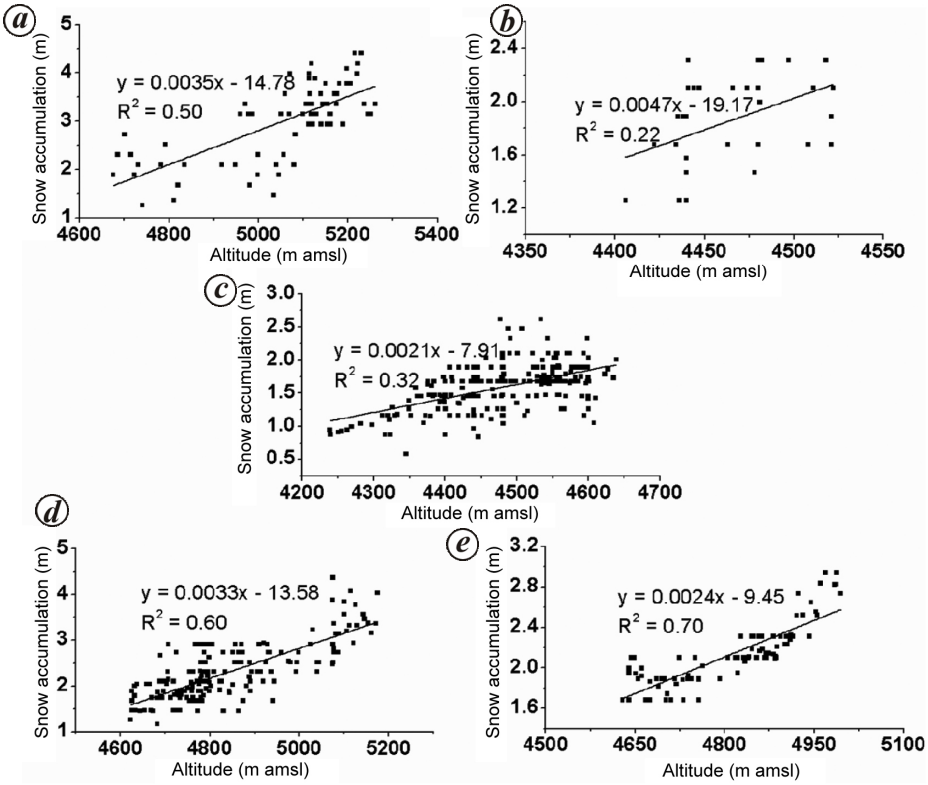

Figure 10. Scatter plot of altitude-wise variation of snow accumulation on Samudra Tapu glacier. ***a***, North glacier (R^2 = 0.50, year 2009); ***b***, Common glacier (R^2 = 0.22, year 2009); ***c***, Common glacier (R^2 = 0.32, year 2010); ***d***, North glacier (R^2 = 0.60, year 2010); ***e***, South glacier (R^2 = 0.70, year 2010).

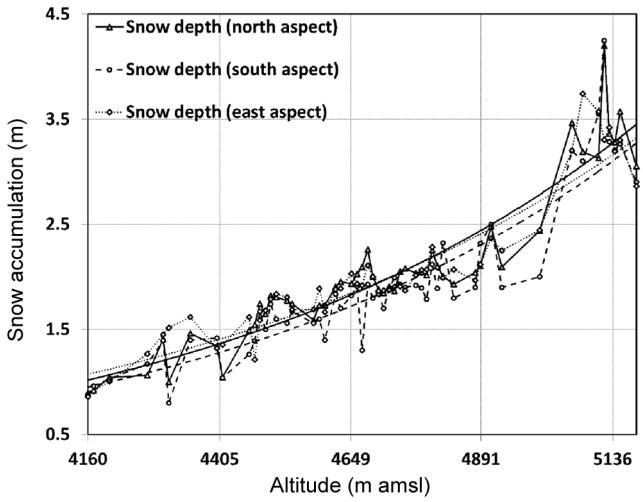

Figure 11. Variation of accumulated snow with altitude at the north, south and east aspects of Samudra Tapu glacier for 2010.

decrease with increase in terrain slope for each altitude class (Figure 12). The negative gradient was observed to be maximum for the lowest altitude class (4300–4500 m) and minimum for the highest altitude class (4900–5100 m). Statistically significant negative correlation was found (r = –0.97; significant at 1% level) between mean snow accumulation and slope for the lower altitude class (4300–4500 m). Furthermore, snow accumulation was observed to be comparatively lower in this class. This lower altitude class falls in the ablation area. In this altitude range because of lesser snow deposition, the role of slope is more prominent in the snow accumulation pattern.

However, for the highest altitude class (4900–5100 m), which lies in accumulation zone of the glacier all of its slopes are completely covered with snow. Statistically insignificant correlation between snow accumulation and slope was found (r = –0.21). This indicates that variation in snow accumulation with slope is not significant for highest altitude class.

Annual difference in snow accumulation: Differences in snow accumulation on the glacier between the years 2009 and 2010 were found from the observations made on the same date, i.e. 22 March. For estimation of these differences, the snow accumulation information from common GPS coordinates of survey data from both the years was selected. Figure 13 *a* shows the differences in snow accumulation between 2009 and 2010 for a part of the Samudra Tapu glacier. It was observed that accumulated snow was low in 2010 compared to that in 2009 in most of the area. Figure 13 *b* shows the accumulated snow depth data comparison for some of the common coordinates. The result was validated using the cumulative snowfall data of 2009 and 2010 (Figure 14) recorded at

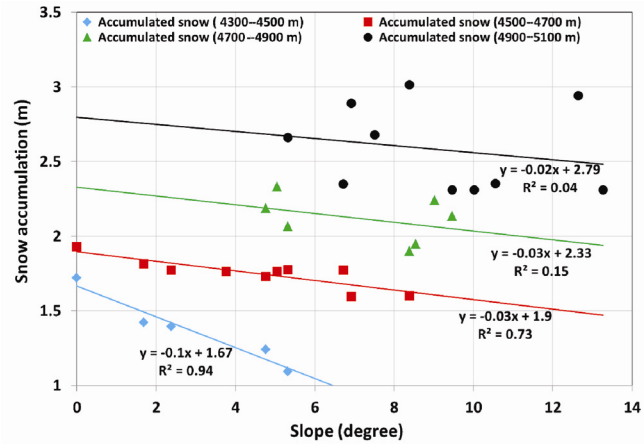

Figure 12. Variation of accumulated snow with terrain slope for different altitude ranges of Samudra Tapu glacier for 2010.

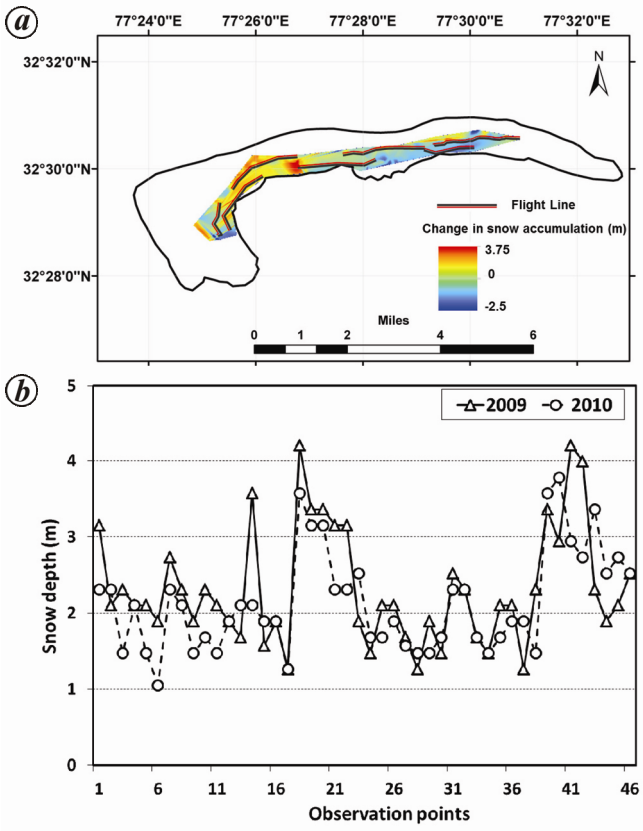

Figure 13. ***a***, Changes in the snow accumulation values as estimated from airborne GPR data between 2009 and 2010 for a part of Samudra Tapu glacier. ***b***, Comparison of snow accumulation values estimated using airborne GPR of the same geographic coordinates in 2009 and 2010 of Samudra Tapu glacier.

snow-meteorological observatory, Patseo[50]. This shows that the retrieved data using GPR can identify change in snow accumulation pattern in a glacier.

Snow water equivalent of glacier-accumulated snow: The SWE of the complete glacier was estimated for 2010. The area of Samudra Tapu glacier is approximately

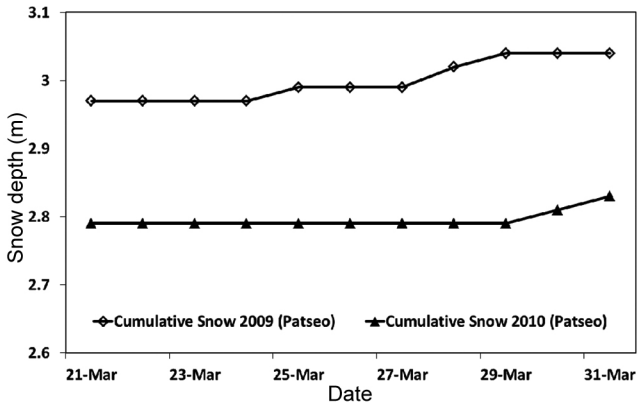

Figure 14. Cumulative snowfall data measured manually at the snow and metrological field observatory (Patseo) in 2009 and 2010 during the same period of airborne survey.

41.06 sq. km. The average value of estimated snow depth over the glacier ice was found to be ~2.48 m using GPR surveyed data and the average snow density from the field observations was 241 kg m^{-3}. The total volume of snow on the glacier was found to be ~0.102 km^3 and the corresponding average SWE was ~0.597 m.

In order to observe the difference of SWE between 2009 and 2010, common glacier area of 6.86 sq. km extending between altitude 5200 and 4400 m was selected. For this area, GPR-estimated average snow depth was 2.23 and 2.06 m for 2009 and 2010 respectively. The snow densities measured at the field observatory were 280 and 240 kg m^{-3} for 2009 and 2010 respectively (Table 2). The estimated average SWE for 2009 was 0.624 m and for 2010 it was 0.496 m, which shows a reduction of 0.128 m. For the same period, the reduction in SWE at field observatory Patseo was 0.159 m (ref. 50). Further, the calculated snow volume over the glacier for 2009 and 2010 was 0.0153 and 0.0141 km^3 respectively. This shows a reduction of 0.0012 km^3 in snow volume of the glacier common area in 2010, compared to 2009. Considering the same rate of decrease for the complete glacier, a reduction of 0.0072 km^3 in snow volume is estimated between 2009 and 2010.

Conclusion

In this study we report the application of airborne GPR technique for snow accumulation measurements carried out in the mountainous terrain of the Indian Himalaya. GPR surveys were conducted in March 2009 and 2010 at Samudra Tapu glacier, to estimate the snow accumulation. A kriging-based geostatistical interpolation method was used to generate spatial snow accumulation map from the GPR-collected data. The accumulated snow depth varied from 2.25 to 4.34 m in the accumulation zone, and 0.72 to 2.25 m in the ablation zone of the glacier. The temporal change in snow accumulation was

Table 2. Measured and derived snowpack properties during 2009 and 2010

	Snow properties				
Surveyed year	Snow density (kg m^{-3})	Snow dielectric	Snow depth (m)	Snow water equivalent (m)	Snow volume (km^3)
2009	280	1.60	2.23	0.624	0.0153
2010	240	1.53	2.06	0.496	0.0141

analysed for two consecutive years (2009 and 2010) for the common surveyed area of Samudra Tapu glacier. The GPR-estimated average accumulated snow depth was 2.23 m for 2009 and 2.06 m for 2010. In addition the corresponding average SWE was estimated to be 0.624 and 0.496 m for 2009 and 2010 respectively. Decreasing pattern in snow depth was also observed at the validation site for the same period. In 2010, the total volume of snow accumulated over the glacier ice was estimated to be ~0.102 km^3. From the analysis, a reduction of 0.0072 km^3 in snow volume was observed between 2009 and 2010.

Further, the snow accumulation data over the glacier were analysed with various topographical parameters such as altitude, aspect and slope. In general, the accumulated snow depth increased with altitude throughout the glacier. However, accumulated snow depth was found to be poorly correlated at lower altitudes compared to higher altitudes. Furthermore, high snow accumulation was observed in the north and east aspects compared to the south aspect. Snow accumulation was found to decrease with increase in the terrain slope for different altitude ranges. The analysis of snow accumulation with respect to the above parameters may help in the estimation of snow accumulation in other nearby glaciers.

The present study provides snow distribution pattern over the glacier at very high spatial resolution (~7 m). Such airborne GPR surveys along with more field sampling sites can improve the prediction of water availability from larger areas. In future, to improve the accuracy of estimated snow depth and SWE, we suggest the use of pre-installed sensors in the study area.

1. Bolch, T. *et al.*, The state and fate of Himalayan glaciers. *Science*, 2012, **336**, 310–314; doi: 10.1126/science.1215828
2. Kulkarni, A. V., Bahuguna, I. M., Rathore, B. P., Singh, S. K., Randhawa, S. S., Sood, R. K. and Dhar, S., Glacial retreat in Himalayas using Indian remote sensing satellite data. *Curr. Sci.*, 2007, **92**, 69–74.
3. Lau, W. K. M., Kim, M. K., Kim, K. M. and Lee, W. S., Enhanced surface warming and accelerated snow melt in the Himalayas and Tibetan Plateau induced by absorbing aerosols. *Environ. Res. Lett.*, 2010, 5; doi:10.1088/1748-9326/5/2/025204
4. Cogley, J. G., Present and future states of Himalaya and Karakoram glaciers. *Ann. Glaciol.*, 2011, **52**, 69–73.
5. Gurung, D. R., Kulkarni, A. V., Giriraj, A., Aung, K. S. and Shrestha, B., Monitoring of seasonal snow cover in Bhutan using remote sensing technique. *Curr. Sci.*, 2011, **101**(10), 1364–1370.
6. Vincent, C. *et al.*, Balanced conditions or slight mass gain of glaciers in the Lahaul and Spiti region (northern India, Himalaya) during the nineties preceded recent mass loss. *Cryosphere*, 2013, **7**, 569–582.
7. IPCC, *Climate Change 2014: Mitigation of Climate Change. Contribution of Working Group III to the Fifth Assessment Report of the Intergovernmental Panel on Climate Change* (eds Edenhofer, O. *et al.*), Cambridge University Press, Cambridge, United Kingdom, 2014.
8. Lozej, A. and Tabacco, I., Radio echo sounding on Strandline Glacier, Terra Nova Bay (Antarctica). *Boll. Geofis. Teor. Appl.*, 1993, **35**, 231–244.
9. Holmund, P., Radar measurement of annual snow accumulation rates. *Z. Gletscherkd. Glazialgeol.*, 1996, **32**, 193–196.
10. Marshall, H. P. and Koh, G., FMCW radars for snow research. *Cold Reg. Sci. Technol.*, 2008, **52**, 118–131.
11. Peduzzi, P., Herold, C. and Silverio, W., Assessing high altitude glacier thickness, volume and area changes using field, GIS and remote sensing techniques: the case of Nevado Coropuna (Peru). *Cryosphere*, 2010, **4**, 313–323.
12. Mitterer, C., Heilig, A., Schweizer, J. and Eisen, O., Upward-looking ground-penetrating radar for measuring wet-snow properties. *Cold Reg. Sci. Technol.*, 2011, **69**, 129–138.
13. Williams, R. M., Ray, L. E., Lever, J. H. and Burzynski, A. M., Crevasse detection in ice sheets using ground penetrating radar and machine learning. *IEEE J. Sel. Top. Appl. Earth Obs.*, 2014, **7**, 4836–4848.
14. Schmid, L., Heilig, A., Mitterer, C., Schweizer, J., Maurer, H., Okorn, R. and Eisen, O., Continuous snowpack monitoring using upward-looking ground-penetrating radar technology. *J. Glaciol.*, 2014, **60**, 509–525; doi:10.3189/2014JoG13J084
15. Van Pelt, W. J. J., Pettersson, R., Pohjola, V. A., Marchenko, S., Claremar, B. and Oerlemans, J., Inverse estimation of snow accumulation along a radar transect on Nordenskiöldbreen, Svalbard. *J. Geophys. Res.: Earth Surf.*, 2014, **119**, 816–835; doi:10.1002/2013JF003040
16. Singh, K. K., Datt, P., Sharma, V., Ganju, A., Mishra, V. D., Parashar, A. and Chauhan, R., Snow depth and snow layer interface estimation using GPR. *Curr. Sci.*, 2011, **100**, 1532–1539.
17. Loveson, V. J., Khare, R., Mayappan, S. and Gujar, A. R., Remote-sensing perspective and GPR subsurface perception on the growth of a recently emerged spit at Talashil coast, west coast of India. *GISci. Remote Sensing*, 2014, **51**, 644–661.
18. Forte, E., Dossi, M., Colucci, R. R. and Pipan, M., A new fast methodology to estimate the density of frozen materials by means of common offset GPR data. *J. Appl. Geophys.*, 2013, **99**, 135–145; doi:10.1016/j.jappgeo.2013.08.013
19. Forte, E., Dossi, M., Pipan, M. and Colucci, R. R., Velocity analysis from common offset GPR data inversion: theory and application on synthetic and real data. *Geophys. J. Int.*, 2014, **197**(3), 1471–1483; doi:10.1093/gji/ggu103
20. Colucci, R. R., Forte, E., Boccali, C., Dossi, M., Lanza, L., Pipan, M. and Guglielmin, M., Evaluation of internal structure, volume and mass of glacial bodies by integrated LiDAR and ground penetrating radar (GPR) surveys: the case study of Canin Eastern Glacieret (Julian Alps, Italy). *Surv. Geophys.*, 2015, **36**, 231–525; doi:10.1007/s10712-014-9311-1
21. Machguth, H., Eisen, O., Paul, F. and Hoelzle, M., Strong spatial variability of snow accumulation observed with helicopter-borne

GPR on two adjacent Alpine glaciers. *Geophys. Res. Lett*., 2006, **33**, L13503; doi:10.1029/2006GL026576
22. Sold, L., Huss, M., Hoelzle, M., Andereggen, H., Joerg, P. C. and Zemp, M., Methodological approaches to infer end-of-winter snow distribution on alpine glaciers. *J. Glaciol.*, 2013, **59**, 1047–1059; doi:10.3189/2013JoG13J015
23. Conway, H., Smith, B., Vaswani, P., Matsuoka, K., Rignot, E. and Claus, P., A low frequency ice-penetrating radar system adopted for use from an airplane: test results from Bering and Malaspina glacier, Alaska, USA. *Ann. Glaciol*., 2009, **51**, 93–104.
24. Das, I. *et al.*, Influence of persistent wind-scour on the surface mass balance of Antarctica. *Nature Geosci*., 2013, **6**, 367–371.
25. Bell, R. E. *et al.*, Widespread persistent thickening of the East Antarctic Ice Sheet by freezing from the base. *Science*, 2011, **331**, 1592–1595.
26. Arcone, S. A., Jacobel, R. and Hamilton, G., Unconformable stratigraphy in East Antarctica: Part 1. Large firncosets, recrystallized growth, and model evidence for intensified accumulation. *J. Glaciol*., 2012, **58**, 240–252.
27. Gergen, J. T., Dobhal, D. P. and Kaushik, R., Ground penetrating radar ice thickness measurements of Dokrianibamak (glacier), Garhwal Himalaya. *Curr. Sci.*, 1999, **77**, 169–173.
28. Singh, K. K., Kulkarni, A. V. and Mishra, V. D., Estimation of glacier depth and moraine cover study using ground penetrating radar (GPR) in the Himalayan region. *J. Indian Soc. Remote Sensing*, 2010, **38**, 1–9.
29. Azam, M. F. *et al.*, From balance to imbalance: a shift in the dynamic behavior of Chhota Shigri glacier, western Himalaya, India. *J. Glaciol*., 2012, **58**, 315–324.
30. Singh, S. K., Rathore, B. P., Bahuguna, I. M., Ramnathan, A. L. and Ajai, Estimation of glacier ice thickness using ground penetrating radar in the Himalayan region. *Curr. Sci*., 2012, **103**, 68–73.
31. Negi, H. S., Mishra, V. D., Singh, K. K. and Mathur, P., Application of ground penetrating radar for snow, ice and glacier studies. In Proceedings of the International Symposium on Snow Monitoring and Avalanches, Snow and Avalanche Study Establishment, Manali, 12–16 April 2004.
32. Negi, H. S., Snehmani, Thakur, N. K. and Sharma, J. K., Estimation of snow depth and detection of buried objects using airborne ground penetrating radar in Indian Himalaya. *Curr. Sci.*, 2008, **94**, 865–870.
33. Gusain, H. S., Singh, A., Ganju, A. and Singh, D., Characteristics of the seasonal snow cover of Pir Panjal and Great Himalayan ranges in Indian Himalaya. In Proceedings of the International Symposium on Snow Monitoring and Avalanches, Manali, 12–16 April 2004.
34. Gusain, H. S., Chand, D., Thakur, N. K., Singh, A. and Ganju, A., Snow avalanche climatology of Indian Western Himalaya. In Proceedings of the International Symposium on Snow and Avalanches, SASE Manali, 6–10 April 2009.
35. Sharma, S. S. and Ganju, A., Complexities of avalanche forecasting in Western Himalaya – an overview. *Cold Reg. Sci. Technol*., 2000, **31**, 95–102.
36. Jaedicke, C., Snow mass quantification and avalanche victim search by ground penetrating radar. *Surv. Geophys*., 2003, **24**, 431–445.
37. Daniels, D., *Ground Penetrating Radar – 2nd Edition*, The Institution of Electrical Engineers, London, 2004.
38. Sihvola, A. and Tiuri, M., Snow fork for field determination of the density and wetness profiles of a snowpack. *IEEE Trans. Geosci. Remote Sensing*, 1986, **24**, 717–721.
39. User/Technical Manual of Snow Fork, the Portable Snow Properties Measuring Instrument, Ins. Toimisto Toikka Oy, Hannuntie 18,02360 Espoo, Finland, 2010.
40. Hengl, T., *A Practical Guide to Geostatistical Mapping* (2nd extended edn). 2009; http://spatial-analyst.net/book/system/files/Hengl_2009_GEOSTATe2c1w.pdf
41. Heilig, A., Schneebeli, M. and Eisen, O., Upward looking ground penetrating radar for monitoring snowpack starigraphy. *Cold Reg. Sci. Technol*., 2009, **59**, 152–162.
42. Ambach, W. and Denoth, A., The dielectric behavior of snow: a study versus liquid water content. In *NASA Workshop on Microwave Remote Sensing of Snowpack Properties* (ed. Rango, A.), NASA Conference Publication, 1980, NASA CP-2153, pp. 59–62.
43. Johnson, G. L. and Hanson, C. L., Topographic and atmospheric influences on precipitation variability over a mountainous watershed. *J. Appl. Meteorol*., 1995, **34**, 68–87; doi:10.1175/1520-0450-34.1.68
44. Roe, G. H. and Baker, M. B., Microphysical and geometrical controls on the pattern of orographic precipitation. *J. Atmos. Sci*., 2006, **63**, 861–880; doi:10.1175/jas3619.1
45. Farinotti, D., Magnusson, J., Huss, M. and Bauder, A., Snow accumulation distribution inferred from time-lapse photography and simple modelling. *Hydrol. Process*., 2010, **24**, 2087–2097; doi:10.1002/hyp.7629
46. Asaoka, Y. and Kominami, Y., Spatial snowfall distribution in mountainous areas estimated with a snow model and satellite remote sensing. *Hydrol. Res. Lett*., 2012, **6**, 1–6.
47. Grünewald, T., Bühler, Y. and Lehning, M., Elevation dependency of mountain snow depth. *Cryosphere*, 2014, **8**, 2381–2394, doi:10.5194/tc-8-2381-2014
48. Kirchner, P. B., Bales, R. C., Molotch, N. P., Flanagan, J. and Guo, Q., LiDAR measurement of seasonal snow accumulation along an elevation gradient in the southern Sierra Nevada, California. *Hydrol. Earth Syst. Sci*., 2014, **18**, 4261–4275.
49. Jain, S. K., Goswami, A. and Saraf, A. K., Accuracy assessment of MODIS, NOAA and IRS data in snow cover mapping under Himalayan conditions. *Int. J. Remote Sensing*, 2008, **29**, 5863–5878.
50. SASE Annual Technical Reports, 2009 and 2010, Snow and Avalanche Study Establishment, Manali.

ACKNOWLEDGEMENTS. We thank R. K. Garg, Jimmy Kansal, V. D. Mishra, P. K. Srivastava and M. R. Bhutiyani for technical support, and Ramanand Singh, Karamjeet, Anek and Ashwani for GPR data collection. We also thank the helicopter pilots and crew members for their support in flying over highly rugged mountainous terrain according to our survey requirements.

Received 17 November 2015; revised accepted 9 November 2016

doi: 10.18520/cs/v112/i06/1208-1218